IEEE Access
Multidisciplinary | Rapid Review | Open Access Journal

Received December 27, 2020, accepted January 15, 2021, date of publication January 19, 2021, date of current version January 27, 2021.

Digital Object Identifier 10.1109/ACCESS.2021.3052797

Frequency Regulation of an Isolated Microgrid With Electric Vehicles and Energy Storage System Integration Using Adaptive and Model Predictive Controllers

MISHKAT ULLAH JAN[1], AI XIN[1], (Member, IEEE), HASEEB UR REHMAN[1], MOHAMED ABDELKARIM ABDELBAKY[1,2], SHEERAZ IQBAL[3], AND MUHAMMAD AURANGZEB[1]

[1]State Key Laboratory of Alternate Electrical Power System With Renewable Energy Source, North China Electric Power University, Beijing 102206, China
[2]Department of Electrical Power and Machines Engineering, Faculty of Engineering, Cairo University, Cairo 12613, Egypt
[3]Department of Electrical Engineering, University of Azad Jammu and Kashmir, Muzaffarabad 13100, Pakistan

Corresponding author: Mohamed Abdelkarim Abdelbaky (m_abdelbaky@ncepu.edu.cn)

This work was supported by the Beijing Natural Science Foundation under Grant 3182037.

ABSTRACT Energy storage system (ESS) possesses tremendous potential to counter both the rapid growth of intermittent renewable energy resources (RESs) and provide frequency support to the microgrid (MG). Since the deployment of ESS has overcome the imbalance between generation and consumption, however, their massive cost, as well as degradation tendency, are the restricting considerations that demand alternative solutions to provide stable microgrid operation. To assist ESS, the electric vehicles (EVs) are incorporated into the system. EVs have been gradually commercially viable and considerable focus has been paid to vehicle-to-grid technologies. Appropriate collaboration between ESS and EVs has good capability to manage the frequency irregularities to ensure the efficient operation of the MG. This article presents a novel combination of two control techniques i.e., model predictive control (MPC) and adaptive droop control (ADC), to tackle the frequency regulation issue in the isolated MG, by effectively controlling the ESS and EVs during the large-scale integration of RESs or huge change in load demand. Firstly, the MPC regulates the ESS according to the system frequency deviation, and secondly, the ADC manages the power of EVs according to system specifications by retaining the least possible power for potential usage of EVs. Moreover, an advanced genetic algorithm is applied to tune the MPC and ADC parameters in order to achieve optimized performance. An isolated MG is modeled and verified in MATLAB/Simulink using the above-mentioned control techniques. Further, different case studies are taken into account to validate the combination of ADC and MPC for frequency regulation of an isolated MG. Additionally, the proposed MPC controller is compared with fuzzy logic proportional-integral (FPI) controller and proportional-integral (PI) controller, the MPC provides better performance results as compared with FPI and PI controllers.

INDEX TERMS Electric vehicles, adaptive droop control, energy storage system, model predictive control, frequency regulation, GA optimization technique.

I. INTRODUCTION

In an electrical power grid, one of the biggest challenges is preserving the power balance between power supply and consumption. In other terms, energy production needs to be comparable to the energy consumed. This limitation is to some degree relaxed by the power system's inertia. The system's inertia is defined by a revolving mass of synchronous generating units primarily used in traditional power systems [1], [2]. For instance, if a system encounters failure in one of its generating units by any accident, an imbalance of power is observed due to a substantial fall in the generation. Hence, the other generators attached to the system will try to recover the power deficit faced by the system by increasing their

The associate editor coordinating the review of this manuscript and approving it for publication was Moussa Boukhnifer.

power generation. The generator rotor's kinetic energy has the ability to even the imbalance to some extent by supporting the system to restore its frequency. Moreover, in modern electrical power systems, the overall inertia is inclined towards the reduction due to the increased integration of renewable energy resources (RESs).

Integration of RESs on a large-scale into the power grid contributes to frequency and voltage instabilities [3]. In general, RESs possess no or low inertia, the converters are required for the integration of photovoltaic (PV) system to the grid which doesn't provide inertia to the grid. Similarly, variable frequency converters are required for wind turbines (WT) that again lowers the inertial response of the WT and does not contribute to the grid stability. Subsequently, as RESs penetration increases, the inertia of the power system decreases [4]. As a result, a power grid with a significant degree of renewable energy production has little potential to respond to power imbalances, which are further amplified by the intermittent existence of RESs. The rate of change of frequency increases due to reduced inertia of the power system which leads to the frequency fluctuation in a very short period of time, and the power imbalance resulting in system frequency instability [5].

Frequency is a continually evolving entity in power systems that is determined by the power production and the demand. For the safe operation of the power grid, the system frequency is maintained within the allowable limits. Therefore, various sets of operating standards for frequency are defined independently by the system operators according to their own system specifications. In the majority of Asian countries and European states, the nominal frequency is 50 Hertz (Hz), while in North and South America this value is 60 Hz. The lower allowable limit of the frequency in China is 49.8 Hz and the upper limit is defined as 50.2 Hz. Meanwhile, under normal situations, the operational range of frequency in France, Great Britain, Belgium, and Austria this range is 50 Hz $\pm$ 0.5 Hz [6]. As stated earlier the operational band of frequency in China is small, therefore the inclusion of RES in the electric network needs additional fortification for smooth operation especially in islanded MG. For this purpose, the energy storage system (ESS) is emerged as a vital entity to be deployed in the power network to support the grid and to make possible the realization of microgrid and smart grid.

In certain cases, the implementation of ESS is essential to ensure the adequate and reliable functioning of the MG. The ESS can adapt to load variations and consume surplus electrical power available in the system. Moreover, the power variability of RESs such as solar and wind generation units can be compensated by the deployment of ESS [7]. Similarly, a mixture of various ESSs with different features will provide a reasonable solution to the MG challenges. The electric vehicle (EV) battery storage also known as mobile battery banks is utilized to lessen the burden on the ESS. The microgrid can benefit from the vehicle to grid (V2G) system in terms of frequency control, spinning reserve, load matching, and support to the reactive power [8]–[10]. The existing microgrids primarily depend on huge synchronous generators for regulating the frequency by the adjustment of their active output power. The combination of the ESS and large EVs fleets can be utilized in regulating the frequency of the system rather than using huge synchronous generators through a proper control strategy for battery charge and discharge [11]. The complexity of control will increase dramatically provided the increase in the share of ESS and the rise in the number of EVs. This postures a new obstacle in designing control strategies to regulate the frequency of isolated MG. The application study of various control schemes is explored in literature since their development. The proportional, integral and derivative or commonly known as PID controllers were used due to their simple structure and easy deployment [12]. However, with the passage of time fuzzy controller [13], co-operative control [14], robust [15] and adaptive virtual control [16], virtual droop based synchronous generator [1], and neural network-based [17] techniques were developed for the frequency control of the system. Moreover, the optimization algorithms including ant colony optimization, bat algorithm, particle swarm optimization (PSO), artificial neural network (ANN), and genetic algorithm (GA) were developed to improve the performance of the of these controllers [18]–[20]. These optimization schemes like ANN provides good results in non-linear systems however it has some control limitation to be applicable in PID controller, similarly, the PSO has the propensity to fall into a local optimum [20], [21].

The ESS provides partial power support due to its limited capacity, therefore a cooperative control schemes between the generating units and ESS is essential for smooth operation [14], [22]. ESS is implemented in power system to support RES [4], [23], PV [1], wind [24], [25] to alleviate the frequency irregularities. Different controllers are deployed in MG to regulate the RES and ESS according to system frequency. Furthermore, droop control [1], fuzzy logic [23], co-operative control [14], and MPC [4], [25] are implemented on ESS to provide frequency support to MG. For the deployment of the EVs in MG and their active participation, a lot of research is carried out on designing appropriate controller or control schemes that can effectively control/regulate the EVs storage [14], [15]. The authors proposed droop and modified droop control techniques to regulate the EVs battery according to system frequency deviations [26], [27]. Moreover, in [28] fuzzy PI and adaptive droop control are used to cater to the frequency in isolated MG.

The above authors either use ESS or EVs to address the frequency issues in MG, they didn't consider the combined effect of both ESS or EVs fleets in isolated MG. Moreover, in [28], [29] the control effort to regulate the controller output is too large to be applied in a specific control application.

The contributions of this article are:

- Frequency regulation of an isolated MG comprising RESs, DG, and prosumers is studied in this work, where two separate control techniques MPC and adaptive

droop control (ADC) are employed to regulate the MG power imbalance by effectively controlling the charging/discharging of the ESS and EVs battery system, respectively.
- The proposed control schemes effectively operate and avoid the destabilization of MG from collapsing during the large-scale integration of RESs or huge change in load demand. Moreover, the ADC provides leverage to EVs to retain the desired power for their potential usage.
- An advanced genetic algorithm optimization toolbox-extension for control and modeling (GAOT-ECM) is used to optimize the parameters of the MPC and ADC for optimal operation. Besides, this GAOT-ECM is also used for optimizing the PI and Fuzzy PI controllers, which are utilized for comparisons with the proposed MPC.

This article is divided into five sections, the microgrid model is presented in section II, the proposed control system design in section III, the results and simulations are presented in section IV, and lastly, the conclusion is drawn.

II. MICROGRID MODELING

In order to verify the stable and reliable operation of the microgrid (MG), extensive research has been conducted on it in recent years. As mentioned above, there are many types of MGs with different operational roles. Here, in this study, an isolated MG is studied in order to validate the performance of various controllers on frequency regulation. The main energy sources are diesel generators (DG) and renewable energy sources (RESs), including wind farms and solar photovoltaic systems. Secondly, the prosumers are introduced, which includes the electric vehicles (EVs) and energy storage system (ESS), and finally, the domestic loads are used as the power consumers as shown in Fig. 1. The eq. (1) provides the complete structure of the isolated MG used for frequency regulation, while the detailed information of each part is given next subsections.

$$\underbrace{\Delta P_{DG}}_{diesel\_generators} + \underbrace{\Delta P_{PV} + \Delta P_{wind}}_{renewable\_generator} \pm \underbrace{\Delta P_{EV} \pm \Delta P_{ESS}}_{prosumers} - \underbrace{\Delta P_L}_{load} = \underbrace{M.s + D}_{system\_inertia\_damping} . \underbrace{\Delta f}_{frequency\_deviation} \quad (1)$$

A. RENEWABLE ENERGY RESOURCES

Sunlight and wind energy are available all over the world. Therefore, solar photovoltaic (PV) systems and wind turbines system (WTS) are commonly used for power generation. The PV system comprises an array of PV cells to convert the sunlight into DC power, a converter to boost DC voltages, and an inverter to get the required AC voltages [30]. The generated PV power depends on the solar irradiance, PV panel voltage and current, and PV cell temperature [31]. Due to the ease of installation and ample solar irradiance, the solar PV system is the first option among the RERs to be deployed in isolated

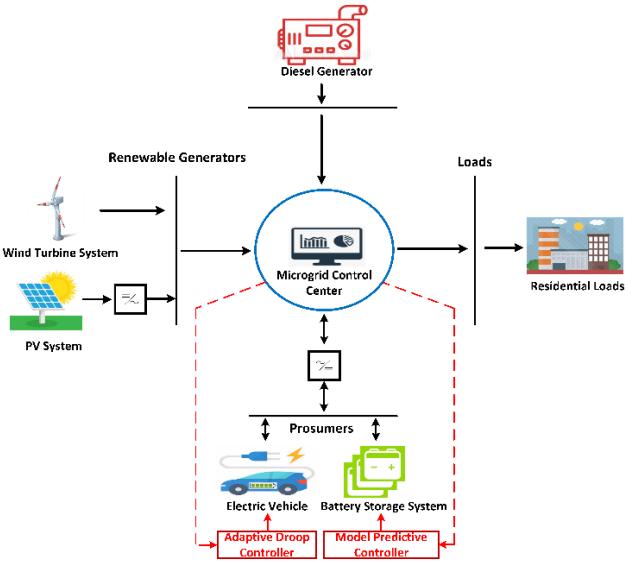

FIGURE 1. The isolated microgrid dynamic model.

MG. The output PV (P_{PV}) can be calculated by eq. (2):

$$P_{PV} = \psi.\varphi.S.(1 - 0.005(T_A - 25)) \quad (2)$$

where ψ, φ and S is the irradiance, conversion efficiency, and effective area of the solar array. While T_A is ambient temperature.

The WTS is comprised of an induction generator which is driven by a wind turbine and further controlled by the governor through the turbine blades' pitch angle (β).

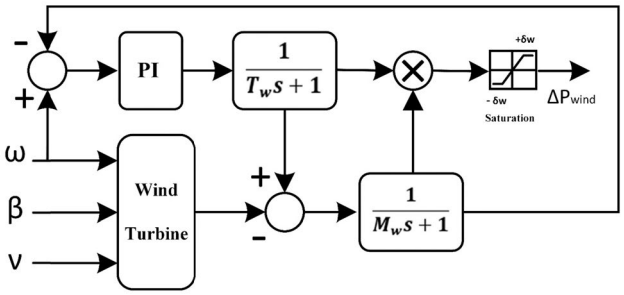

FIGURE 2. The wind turbine system dynamic model.

The inputs to the turbine are wind speed (V) and mechanical speed (ω) of the machine attached to the turbine [32]. In Fig. 2, the output increment in wind turbine system (WTS) is represented by ΔP_{wind}, T_w is the WTS turbine constant and $\pm\delta w$ is the ramp limits [33]. Generally, the WTS output power (P_{wind}) depends technical parameters, which are defined in the following equation [33, 34]:

$$P_{wind} = \frac{1}{2} C_p(\lambda, \beta) A \eta \rho_a V^3 \quad (3)$$

C_p is the capturing efficiency, λ is tip speed ratio and β is the blade pitch angle of the wind turbine, moreover, A, η, ρ_a and V is efficiency, air density, and wind speed, respectively. Moreover, the converters' losses are not included in this work.

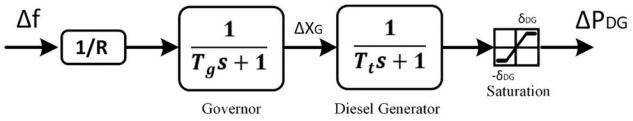

FIGURE 3. The first-order transfer function of diesel generators.

B. DIESEL GENERATOR MODEL

Generally, a diesel generator (DG) is placed in those areas where there is no grid connection or used as an alternative emergency power source to supply power when there occur some faults in the main-grid. Moreover, DG is not only deployed for backup or emergency units, but they have auxiliary functions to supply power to counter the intermittency of RESs in isolated MG. Besides these, the DG has the advantages of fast start-up, high efficiency, and less maintenance cost. Moreover, it has the ability to vary its generation instantly according to the load variations through its power control mechanism. The DG's transfer function is presented in Fig. 3, where the first block is the governor, followed by the DG block and then the saturation block. Based on the frequency deviation (Δf), the governor regulates the state of the valve (ΔX_G), R represents the droop and the increment in the DG output power is given by ΔP_{DG}. In order to meet the power balance, the ramp rate limit ($\pm\delta_{dg}$) determines the rate at which the output power of the DG can be changed. T_t and T_g are the generator and governor time constants, correspondingly.

C. PROSUMERS

The EVs were initially developed in the late 19th century for transportation but due to the advancement in the internal combustion engine vehicles and lack of battery advancement, they were extinct. In 2008, the reemergence of EVs occurred, where they not only provide transportation service but also provide ancillary services to the grid in order to make the modern world clean and green [35]. In order to facilitate a safe and reliable substitution of traditional power sources, EVs are prominent viable assets of the power system, given that their individual responses are fairly aggregated. By controlling the EVs battery (EVBs) system charging/discharging procedure, they can effectively regulate the peak load, increase the grid reliability, indemnify the effect of intermittent RES on-grid fluctuations and manage the frequency instability by the adequately charging and discharging mechanisms.

Moreover, in isolated MG the EVs deliver the vehicle to grid facilities to the MG for frequency stabilization through battery regulation of EVs. Recent studies have shown that EVs are idle most of the time during the day. More specifically, the three folded benefits of EVBs are: (a) they effectively manage the MG frequency by regulating their storage according to system load variations, (b) they provide additional storage to the MG resulting in the decrease in the expanse/cost of consumption by an extra energy storage system, and (c) they also provide economic benefits to the owner

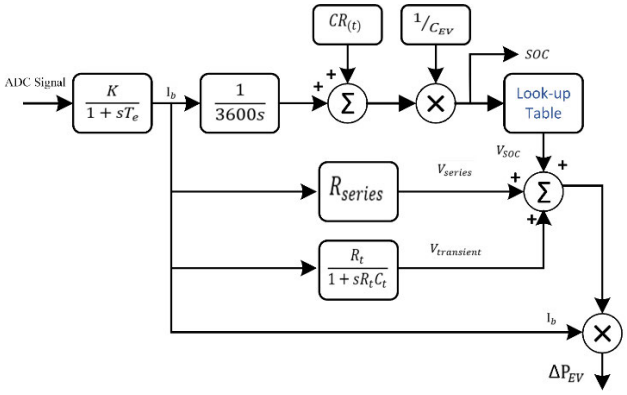

FIGURE 4. First-order transfer function model of an EV battery system.

by selling power during peak hours to MG. The detailed model is explained in [28], [36], is shown in Figure(4). The K, C_{EV} and T_{EV} is the droop, rated capacity and time constant of EV battery, respectively. Moreover, the battery internal characteristics are not studied, as they do not affect the main theme of this work. The increment in the EV output power (ΔP_{EV}) is the difference between the regulation power (P^D_{EV}) and charging power (P^C_{EV}) of the EV ($\Delta P_{EV} = P^D_{EV} - P^C_{EV}$). This ΔP_{EV} is regulated by Δf as given in eq. (4).

$$\Delta P_{EV} = \Delta f . \frac{K_{EV}}{1 + T_{EV} s} \tag{4}$$

Due to its short reaction time and organizational versatility, the energy storage system (ESS) is among the most desirable candidates that provide frequency regulation services in isolated MG. ESS technology can insert a huge amount of electricity into the grid in a limited period due to quick reaction time that can be utilized as virtual inertia [1]. The ESS offers upward / downward control by considering the need to inject/absorb power according to the grid requirements, as comparing to the fast-traditional generation units that are held on-line to provide primary frequency regulation by controlling the power output in case of any frequency deviation event occurs [37].

It's the first line of defense which rescue the isolated MG under load-generation unbalance condition. Normally the ESS operates its state of charge between (SOC) between 20 and 90 because the behavior of the output power of ESS (ΔP_{ESS}) is linearly increased and decreased in this range according to frequency variations. The ESS transfer function is presented in Fig. 5.

III. THE PROPOSED CONTROL SYSTEM DESIGN

A. THE PROBLEM FORMULATION

In this work, an isolated MG is studied to check the effect of both ESS and EVs on the frequency regulation of MG. An adaptive droop control (ADC) technique is used for the regulation of EV's battery (EVB) while an MPC controller is used to manage the energy storage system (ESS) output according to the system frequency deviation. Furthermore,

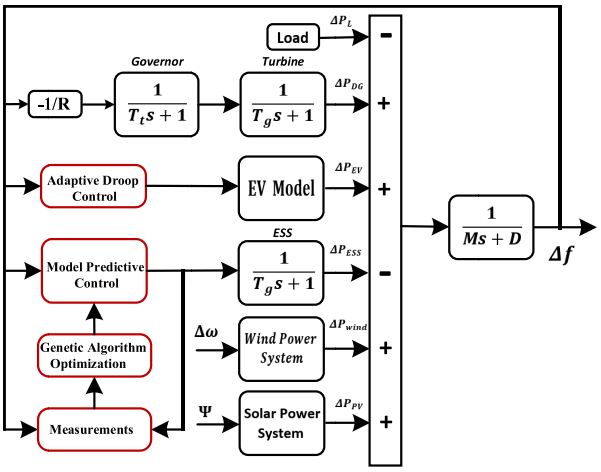

FIGURE 5. A dynamic model of the proposed system.

an advanced genetic algorithm (GA) is employed on the MPC and ADC parameters in order to achieve the optimal solution.

B. FUZZY LOGIC PI CONTROLLER

The proportional-integral (PI) and fuzzy logic PI (FPI) controllers are implemented in order to compare their performance with the model predictive controller (MPC). The inputs to the FPI controller are frequency deviation (Δf) and its derivative ($d\Delta f$) as shown in Fig.6. The fuzzy process consists of fuzzification, fuzzy inference system (FIS), and defuzzification. Fuzzification begins its process on the crisp input data, where the crisp value is mapped to a fuzzy input value dependent on the corresponding membership function.

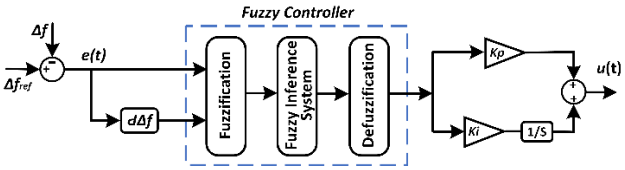

FIGURE 6. Fuzzy PI Controller.

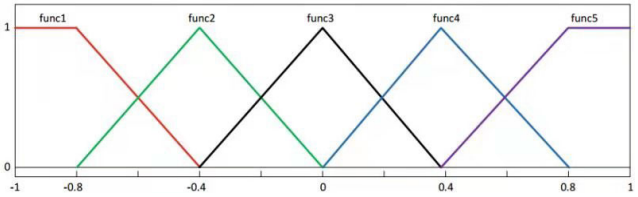

FIGURE 7. Mamdani type FIS output pattern.

The Mamdani-type FIS output variables are presented in Fig. 7. In the next stage, the FIS utilizes the membership functions (MF's) and fuzzy rules to yield the output. Here five fuzzy sets are used to provide 25 rules base for the system as given in Table 1. MF's is comprehended as a contour that portrays the mapping of membership value of every step.

TABLE 1. Fuzzy rule base.

Δf \ $d\Delta f$	*func1*	*func2*	*func3*	*func4*	*func5*
func1	*func1*	*func1*	*func2*	*func2*	*func3*
func2	*func1*	*func2*	*func2*	*func3*	*func4*
func3	*func2*	*func2*	*func3*	*func4*	*func4*
func4	*func2*	*func3*	*func4*	*func4*	*func5*
func5	*func3*	*func4*	*func4*	*func5*	*func5*

The MF's are spread from negative big (*func1*) to positive big (*func5*), encompassing negative small (*func2*), positive small (*func4*), and zero (*func3*). IF-THEN function is used to map the fuzzy rules as given in Table 1.

IF Δf is *func5* **AND** $d\Delta f$ is *func4*, **THEN** output is *func5*.

Moreover, the FL approach is described as a set of principles and rules which are mathematically defined by membership degrees instead of binary logic [38]. The recently developed genetic algorithm optimization technique (GAOT-ECM) is implemented to optimized the controllers for better results under unenviable situations based on eq. (24) [19].

C. ADAPTIVE DROOP CONTROLLER FOR THE ELECTRIC VEHICLE

Before connecting to MG, the initial state of charge (S^{in}), the desired state of charge (S^{d}) and the time of arrival (t^{arr}) of the EV is calculates. The total power of the EVs (P_{EV}^{T}) is the resultant of the power possessed by EVB during charging (P_{EV}^{c}) and provided during regulation (P_{EV}^{d}) as given in the following set of equations.

$$\begin{cases} P_{EV}^{T} = P_{EV}^{d} - P_{EV}^{c} \\ P_{EV}^{d} = P_{EV}^{max} K_{EV}^{d} \\ P_{EV}^{c} = P_{EV}^{max} K_{EV}^{c} \end{cases} \tag{5}$$

where K_{EV}^{d} and K_{EV}^{c} is discharging and charging droops of the EVB, respectively. The EV regulate the batteries SOC by I_{reg} current. It is calculated by the difference between the S^{d} and S^{in}, the total plugin time (t^{p}), the rated capacity (C_{EVB}) and EVB voltage (V_{EVB}). This regulation current is solely dependent upon the former three parameters, as the last two parameters remain constant. The mathematical equation of I_{reg} is given below:

$$I_{reg} = \left(\frac{S^{d} - S^{in}}{t^{p}} \right) . \frac{C_{EVB}}{V_{EVB}} \tag{6}$$

As the EVs provide supplementary support to isolated MG, so the first goal is to charge the EVBs to their desired level (S^{d}). The adaptive droop controller (ADC) manages the K_{EV}^{c} and K_{EV}^{d} based on the following set of equations.

$$\text{If } S^{in} \leq S^{min} \begin{cases} K_{EV}^{c} = K_{max} \\ K_{EV}^{d} = 0 \end{cases} \tag{7}$$

If $S^{min} \leq S^{in} \leq S^{d}$, then

$$\begin{cases} K_{EV}^{c} = 0.8K_{max}\left(1+\sqrt{\dfrac{S^{d}-S^{in}}{S^{in}-S^{min}}}\right) \\ K_{EV}^{d} = 0.2K_{max}\left(1-\sqrt{\dfrac{S^{d}-S^{in}}{S^{in}-S^{min}}}\right) \end{cases} \tag{8}$$

If $S^{d} \leq S^{in} \leq S^{max}$, then

$$\begin{cases} K_{EV}^{c} = 0.5K_{max}\left(1-\sqrt{\dfrac{S^{in}-S^{d}}{S^{max}-S^{in}}}\right) \\ K_{EV}^{d} = 0.5K_{max}\left(1+\sqrt{\dfrac{S^{in}-S^{d}}{S^{max}-S^{in}}}\right) \end{cases} \tag{9}$$

where S^{in}, S^{min}, S^{d}, S^{max} and S^{rated} are the initial, minimum, desired, maximum, and rated *SOC* of the EVB, respectively. For better performance the *SOC* of EVB is classified into four distinct zones as $0 < S^{min} < S^{d} < S^{max} < S^{rated}$. These zones are vital as the EV batteries *SOC* show a linear behaviour between S^{min} and S^{max}, which is set at twenty and ninety percent, respectively. Moreover, to preserve the EVBs health and avoid their degradation, S^{d} is introduced. The S^{d} is that mark until which the EVB *SOC* must be preserved for future transportation usage of the EV. The *ADC* regulates the EVBs power according to the frequency deviation (Δf) in the MG and, the S^{in} of EVBs based on the eq. (7,9). The pictorial representation of *ADC* is presented in Fig. 8.

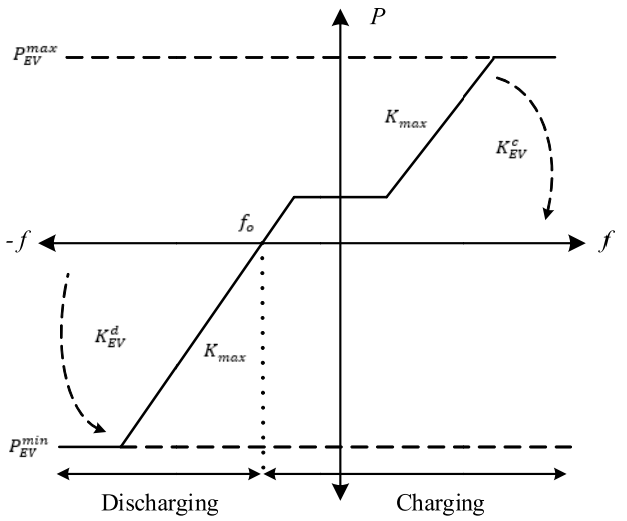

FIGURE 8. EVBs power regulation based on frequency deviation.

The EV having S^{in} less than S^{min} is put in charging state, until and unless the S^{in} is greater than S^{min}, the K_{EV}^{d} is zero as the EVB doesn't provide power to MG in this state. Moreover, when S^{in} lies between the S^{min} and S^{d}, the *ADC* will observe the Δf situation at the isolated MG. When the Δf is positive, the K_{EV}^{c} charging droop is set greater for fast charging. However, when Δf is negative, the EVBs having greater power, releases energy in order to cater the system frequency.

The parameter k_{max} of the ADC is optimized by the genetic algorithm, which is investigated in the next subsection B.2.

D. MPC CONTROL DESIGN FOR THE ENERGY STORAGE SYSTEM

MPC is implemented here to regulate the input signal to ESS according to the frequency deviation. The continuous state-space model of the complete microgrid in Fig. 5 can be expressed by Eq. (10):

$$\begin{aligned} \dot{x} &= Ax + Bu \\ y &= Cx \end{aligned} \tag{10}$$

where A,B, C are the continuous state-space matrices and these matrices are presented as follows A, B, and C, as shown at the bottom of the next page. The input is $u = [\Delta u_{ESS}]$, the output is $y = [\Delta f]$, the states are defined as follows:

$$x = [\Delta P_{ESS}\ \Delta P_{wind}\ \Delta P_{DG}\ \Delta X_G\ \Delta f\ \Delta\omega\ \Delta P_L\ \Delta P_{EV}\ \Delta P_{PV}]^{T}$$

The optimization phase and state estimation phase are the two main model predictive control (MPC) operation phases as presented in Fig. 9 [39]. The current state variables State estimation can be obtained by measuring the, in which the prediction model in eq. (11) is utilized to estimate the future state variables prediction.

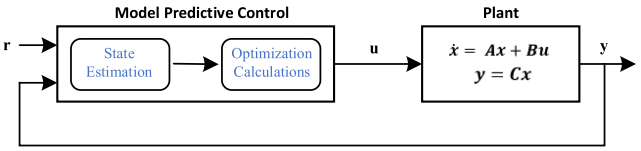

FIGURE 9. Model predictive control operation.

The discrete state-space model of the continuous model in (6) with sampling time T_s, which is utilized to design the MPC, can be stated by:

$$\begin{aligned} x(k+1) &= A_d x(k) + B_d u(k) \\ y(k) &= C_d x(k) \end{aligned} \tag{11}$$

where A_d, B_d, C_d are the discrete state-space matrices.

The predictive control design is to calculate the predicted system output with future control inputs as the adaptable variables. By choosing the new states vectors as $x_a(k) = [\Delta x(k)^{T} y(k)]^{T}$. The following augmented model is utilized for the MPC design:

$$\begin{bmatrix} \Delta x(k+1) \\ y(k+1) \end{bmatrix} = \begin{bmatrix} A_d & 0 \\ C_d A_d & 1 \end{bmatrix} \begin{bmatrix} \Delta x(k) \\ y(k) \end{bmatrix} + \begin{bmatrix} B_d \\ C_d B_d \end{bmatrix} \Delta u(k)$$
$$y(k) = \begin{bmatrix} 0\ I \end{bmatrix} \begin{bmatrix} \Delta x(k) \\ y(k) \end{bmatrix} \tag{12}$$

The above-augmented model can be put in the following compact form:

$$\begin{aligned} x_a(k+1) &= A_a x_a(k) + B_a \Delta u(k) \\ y(k) &= C_a x_a(k) \end{aligned} \tag{13}$$

where A_a, B_a, C_a represent the augmented model's state-space matrixes. Typically, at each sample k: the future control trajectory is based on the current input measurements ΔU. Using the augmented model in eq. (13), the predicted states for future N_p (prediction horizons) are getting based on the measured states $x(k)$ at sample k as follows:

$$\begin{aligned}
x_a(k+1\,|\,k) &= A_a x_a(k) + B_a \Delta u(k)\\
x_a(k+2\,|\,k) &= A_a^2 x_a(k) + A_a B_a \Delta u(k) + B_a \Delta u(k+1)\\
&\vdots\\
x_a\left(k+N_p\,|\,k\right) &= A_a^{N_p} x_a(k)\\
&\quad + A_a^{N_p-1} B_a \Delta u(k) + \ldots\\
&\quad + A_a^{N_p-N_c} B_a \Delta u(k+N_c-1)\\
x_a(k+2\,|\,k) &= A_a x_a(k+1\,|\,k) + B_a \Delta u(k+1)
\end{aligned} \tag{14}$$

The control action of MPC is predicted for future N_c (control horizons) samples. The future outputs trajectories are defined based on the predicted states, as follows:

$$\begin{aligned}
y(k+1\,|\,k) &= C_a x_a(k_i+1\,|\,k)\\
y(k+1\,|\,k) &= C_a A_a x_a(k) + C_a B_a \Delta u(k)\\
y(k+2\,|\,k) &= C_a A_a x_a(k+1\,|\,k) + C_a B_a \Delta u(k+1)\\
y(k+2\,|\,k) &= C_a A_a^2 x_a(k) + C_a A_a B_a \Delta u(k)\\
&\quad + C_a B_a \Delta u(k+1)\\
&\vdots\\
y\left(k+N_p\,|\,k\right) &= C_a A_a^{N_p} x_a(k)\\
&\quad + C_a A_a^{N_p-1} \Delta u(k) + \ldots\\
&\quad + C_a A_a^{N_p-N_c} B_a \Delta u(k+N_c-1)
\end{aligned} \tag{15}$$

To collect all the equations at the different samples, the following vectors are defined:

$$\begin{aligned}
Y = [&y(k+1\,|\,k)\, y(k+2\,|\,k)\, y(k+3\,|\,k)\\
&\ldots\ldots y\left(k+N_p\,|\,k\right)]^T
\end{aligned}$$

$$\begin{aligned}
\Delta U = [&\Delta u(k) \Delta u(k+1) \Delta u(k+2)\\
&\ldots\ldots \Delta u(k+N_c-1)]^T
\end{aligned}$$

By combining all equations in (12) and (13) the following equation can be written for the predicted output:

$$Y = F x_a(k) + \emptyset \Delta U \tag{16}$$

where F, as shown at the bottom of the page. At each sample k, the following objective function in terms of ΔU, Y, and X is minimized as follows:

$$J = (R_s - Y)^T (R_s - Y) + \Delta U^T \bar{R} \Delta U \tag{17}$$

where $R_s = \begin{bmatrix} 1 & 1 & \cdots & 1 \end{bmatrix}^T_{1*N_p} * r_s$, $\bar{R} = Identity(N_c, N_c) * k_{mpc}$. $\bar{R}$ is supposed positive definite matrices. The R_s is the reference input, the $\bar{R}$ is weight matrix on ΔU over the predictive horizon.

The objective is designed to find the best control parameter vector of ΔU. This can happen by converting the previous objective function in a quadratic form in terms only on ΔU. By substituting Equations (11) into Eq. (12), the resulting objective function will be as following:

$$\begin{aligned}
J = &(R_s - F x_a(k))^T (R_s - F x_a(k))\\
&-2\Delta U^T \emptyset^T (R_s - F x_a(k)) + \Delta U^T \left(\emptyset^T \emptyset + \bar{R}\right) \Delta U
\end{aligned} \tag{18}$$

where $(R_s - F x_a(k))^T (R_s - F x_a(k))$ can be ignored as it is not related to ΔU.

The objective function's derivative J are given as follows:

$$\frac{\partial J}{\partial \Delta U} = -2\phi^T (R_s - F x(k_i)) + 2\left(\emptyset^T \emptyset + \bar{R}\right) \Delta U \tag{19}$$

The necessary condition to find the minimum J can be obtained as follows:

$$\frac{\partial J}{\partial \Delta U} = 0 \tag{20}$$

$$A = \begin{bmatrix}
-1/T_{ESS} & 0 & 0 & 0 & 0 & 0 & 0 & 0 & 0\\
0 & -1/T_w & 0 & 0 & 1/T_w & 0 & 0 & 0 & \\
0 & 0 & -1/T_g & 0 & -1/(R*T_g) & 0 & 0 & 0 & 0\\
0 & 0 & 1/T_t & 0 & 0 & 0 & 0 & 0 & 0\\
-1/DH & 1/DH & 0 & -1/DH & -D/DH & 0 & -1/DH & 1/DH & 1/DH\\
0 & 0 & 0 & 0 & 0 & 0 & 0 & 0 & 0\\
0 & 0 & 0 & 0 & 0 & 0 & 0 & -1/T_{EV} & 0\\
0 & 0 & 0 & 0 & 0 & 0 & 0 & 0 & 0
\end{bmatrix}$$

$$B = \begin{bmatrix} 1/T_{ESS} & 0 & 0 & 0 & 0 & 0 & 0 & 0 & 0 \end{bmatrix}^T;$$

$$C = \begin{bmatrix} 0 & 0 & 0 & 0 & 1 & 0 & 0 & 0 & 0 \end{bmatrix}$$

$$F = \begin{bmatrix} C_a A_a \\ C_a A_a^2 \\ C_a A_a^3 \\ \vdots \\ C_a A_a^{N_p} \end{bmatrix}, \emptyset = \begin{bmatrix}
C_a B_a & 0 & 0 & \cdots & 0\\
C_a A_a B_a & C_a B_a & 0 & \cdots & 0\\
C_a A_a^2 B_a & C_a A_a B_a & C_a B_a & \cdots & 0\\
\vdots & \vdots & \vdots & \cdots & \vdots\\
C_a A_a^{N_p-1} B_a & C_a A_a^{N_p-2} B_a & C_a A_a^{N_p-3} B_a & \cdots & C_a A_a^{N_p-N_c} B_a
\end{bmatrix}.$$

From eq. (19-20), the optimal control signal solution is associated with the state variable $x(k_i)$ and the setpoint reference $r_s(k_i)$ as follows:

$$\Delta U = \left(\emptyset^T \emptyset + \bar{R}\right)^{-1} \emptyset^T (R_s - Fx\,(k_i)) \tag{21}$$

where $R_s = \begin{bmatrix} 1 & 1 & \cdots & 1 \end{bmatrix}^T_{1*N_p} * r_s$, $\bar{R} = Identity\,(N_c, N_c) * k_{mpc}$.

The final input rate signal Δu (with receding control policy) is expressed as follows:

$$\Delta u_{final} = \begin{bmatrix} 1 & 0 & 0 & \cdots & 0 \end{bmatrix}_{N_c*1} * \Delta U \tag{22}$$

The final input signal u is expressed as follows:

$$u_{final} = u_0 + \Delta u_{final} \tag{23}$$

where u_0 represents the previous control input. The parameter k_{mpc} of the MPC is optimized by the genetic algorithm, which is investigated in the following subsection.

GENETIC ALGORITHM OPTIMIZATION OF THE MPC PARAMETERS

GA is an optimization technique that can perform fast searches in a huge amount of ambiguous or partial data set with an in-built structure that permits parallelization. As GA has an empirical nature, therefore, it can integrate into the limits of the fitness function, performance indexes, and objectives which are not essentially well-defined in a good way. Moreover, more restrictions are added to state a possible entity as a fit solution the given issues are not a computational burden. In a modern study, GA has been used to cater to issues in different fields. Their popularity keeps increasing due to their ease of use, effectiveness, or applicability. GA has been effectively used in the control system [40] with feedforward and feedback controllers, parameter approximation [41], and modeling [42]. Furthermore, GA has been applied in several other areas for different issues as a standalone technique [19], distributed control system [43], in coordination with new state of the art techniques such as neural networks [44], or virtual synchronous generator [45]. An advanced GA is used to get the optimized results of the droop controller for frequency regulation.

The following series of steps are executed to run an evolutionary algorithm (EA) as given in Fig. 10:

(a) Initialization of solution population, followed by the evaluation of fitness function; (b) given that a formerly declared termination state is not reached, for each generation based on their measured fitness, certain individuals are chosen and recombined to produce offspring; and (c) the fitness of the current population is assessed to be included in the next period. EAs conduct simultaneous searches in multiple directions in order to find the solution within a given population by assessing the adequacy of each entity, as a fitness variable calculated using a parameter or index that models the desired target. In addition, in order to locate the desired solution within a given population of possible solutions, multi-criteria searches can be carried out.

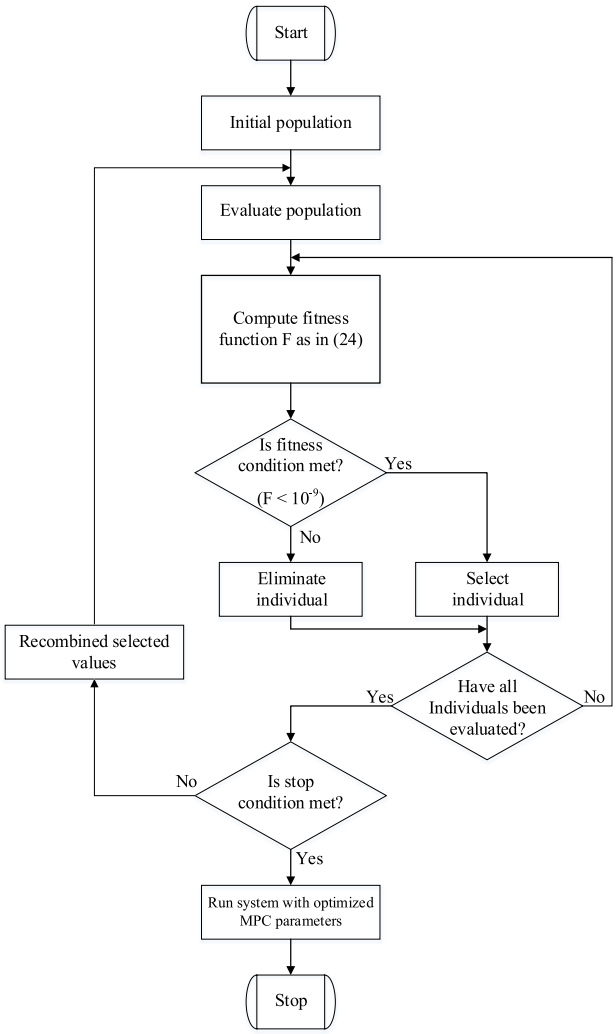

FIGURE 10. The advanced genetic algorithm steps.

The definition of the fitness function is problem-specific, used to model the general goal of the treatment, while its aim is to remove insufficient solutions from the gene pool. This feature returns the value of the output criterion (for example, the minimization index) used to pick new-generation parents. The efficiency of the entire algorithm is given by the fitness during its run of the best population, or by the fitness of the returned final solution.

IV. SIMULATION RESULTS

The isolated MG is modeled in MATLAB/Simulink (R2019b), the parameters' values of the microgrid are defined in Table 2. The proposed controllers are validated for four cases based on the addition of generating entities. Initially, the effectiveness of model practice control (MPC) is compared with the proportional-integral (PI) controller and fuzzy PI (FPI) [29] by considering the energy storage system (ESS). In the second case, renewable energy resources are added, the electric vehicles are considered along with other entities. Lastly, the real data of wind and solar are used for

TABLE 2. System parameters.

Parameters	Value	Parameters	Value
DG rated power (MW)	10	WTS inertia constant M_w (s)	5
ESS rated power (MW)	5	WTS time constant T_w (s)	1.5
PV rated power (MW)	3	WTS K_{iw} parameter	3.6
WTS rated power (MW)	5	WTS K_{pw} parameter	5.7
Battery Capacity of EVs (kWh)	66.2	EV gain K_{EV}	1
Damping Constant D (pu/Hz)	0.015	EV battery time constant T_{EV}(s)	1
Droop coefficient R (Hz/pu)	3	S^{min}, S^{max}	0.2, 0.9
DG generator time constant T_g (s)	0.08	S^d	0.6
DG turbine time constant T_t (s)	0.4	DH (s)	0.1667

TABLE 3. Genetic algorithm parameters.

Parameters	Value	Parameters	Value
Variables	$K_p, K_i, K_{mpc}, K_{max}$	Populations	50
Lower Bounds	[0 0 0 0]	Iterations	50
Upper Bounds	[10 10 10 10]	Crossover	Single Point
Mutation	80%		

the validation of MPC and adaptive droop control (ADC) techniques. The MPC's prediction horizon is $N_p = 10$ and control horizon is $N_c = 2$. The genetic algorithm parameters are represented in Table 3. The proposed fitness function is given in eq. (24).

$$Fitness\ function = 0.001 * \left((U_{ESS})^2 + (U_{ADC})^2\right) + 0.999 * (|\Delta f|) \quad (24)$$

After performing optimization, the MPC and ADC parameters after GA optimization are k_{mpc}= 0.1 and k_{max}= 0.5, respectively. For comparison purposes, the PI controller is optimized using the advanced GA. The cost function and the options of the GA are the same as used for the MPC parameters optimization. In industrial applications the upper and lower bounds of the PI parameters (K_p and K_i) are kept between 0 and 10. The final parameters of the PI controller after optimization are K_p= 1.16 and K_i= 1.74.

A. CASE 1

In the first case, a load disturbance (ΔP_L) of 0.02 p.u. is applied at a time (t = 1s) to validate the performance of the proposed MPC as shown in Fig 11(a). Simulations are done on the proposed model by considering the energy storage system. The control signals (U_{ESS}) which regulates the ESS is presented in Fig 11(b).

Fig. 11(c) shows the output of ESS power (ΔP_{ESS}). The frequency variations (Δf) of the isolated MG by deploying PI, FPI, and MPC controllers are given in Fig. 11(d). From the results, it is evident that the overshoot, settling time, and

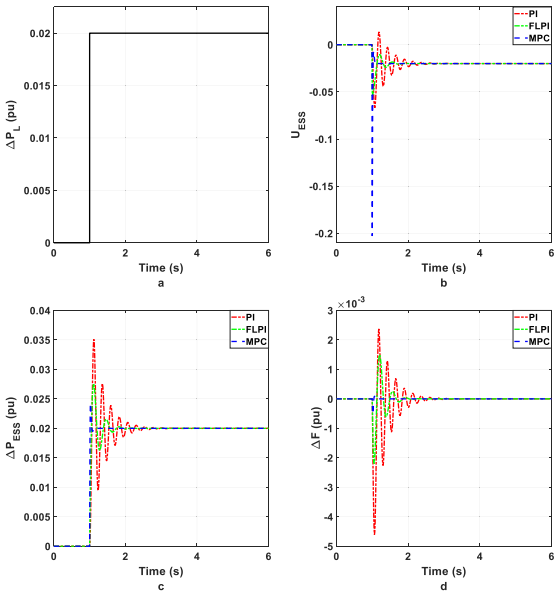

FIGURE 11. The performance results for ESS for load variations by PI, FPI, and MPC controllers. (a) step-change load variation in p.u. (b) The input signal of ESS. (c) the power of the ESS (d) The frequency response.

frequency minimization of MPC is much better than PI and FPI controllers.

B. CASE 2

Here, variations in wind power (ΔP_{wind}) and solar PV system (ΔP_{PV}) are considered in order to demonstrate the performance of the proposed controllers. Moreover, the unit step load ΔP_L is increased to 0.2 p.u. as shown in Fig. 12(a), where Fig. 12(b) depicts the input U_{ESS} to the ESS under this variable load, which regulates the output power of ESS (Fig. 12(c)) according to the system needs. The wind generator speed and the irradiation of the PV cell (Fig. 12(i)), which are responsible for the wind and the PV output power generation are presented in Fig. 12(k). The Δf restoration of the system by using the PI, FPI, and MPC controllers are given in Fig.12(d). The PI surpasses $\pm 0.02\Delta f$ at $t = 1sec$ and $t = 7.5sec$, similarly, the optimized FPI crosses this limit at $t = 1sec$.

Although all the controllers bring back the Δf to operating value, however, the overshoot, settling time, and frequency minimization performance of the optimized MPC is better than the remaining two controllers.

C. CASE 3

In this case, the same load variation, the ESS, and the RESs penetration are used, however, the electric vehicle batteries (EVBs) are the additional entity included checking the MG frequency stability. The input signal (U_{EV}) which regulates the EVBs, the voltage, current and the power of the EVs are given in Fig. 13(e), 13(f), 13(g), and 13(h), respectively. Initially, the ESS tries to charge its battery storage, but at $t = 1sec$ a step load change of 0.2 p.u. is applied. As the EVs connected to the system tries to achieve their desired SOC

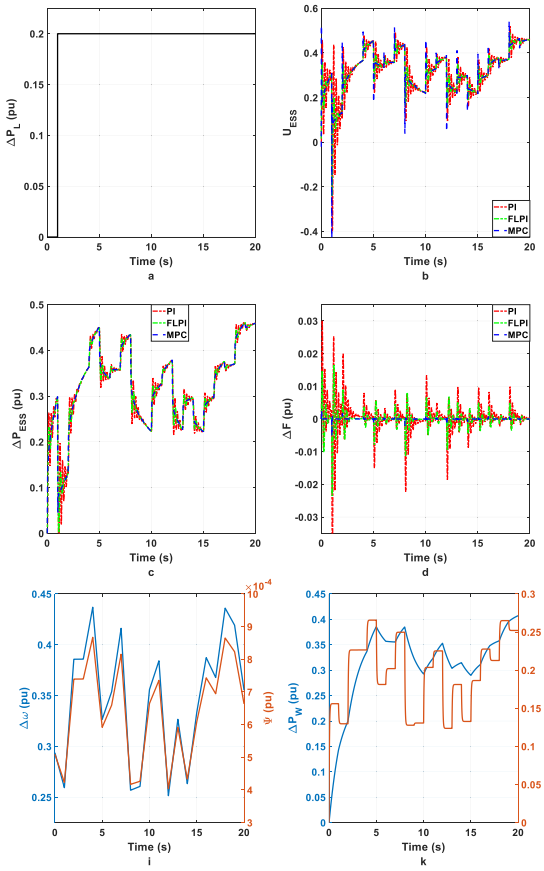

FIGURE 12. The performance results for ESS/EV for load variations with RESs penetration by PI/*ADC*, FPI/*ADC*, and MPC/*ADC* controllers. (a) step-change load variation in p.u. (b) The input signal of ESS. (c) the power of the ESS (d) The frequency response (i) The generator speed and the irradiation of the PV cell (k) The wind and the PV output power.

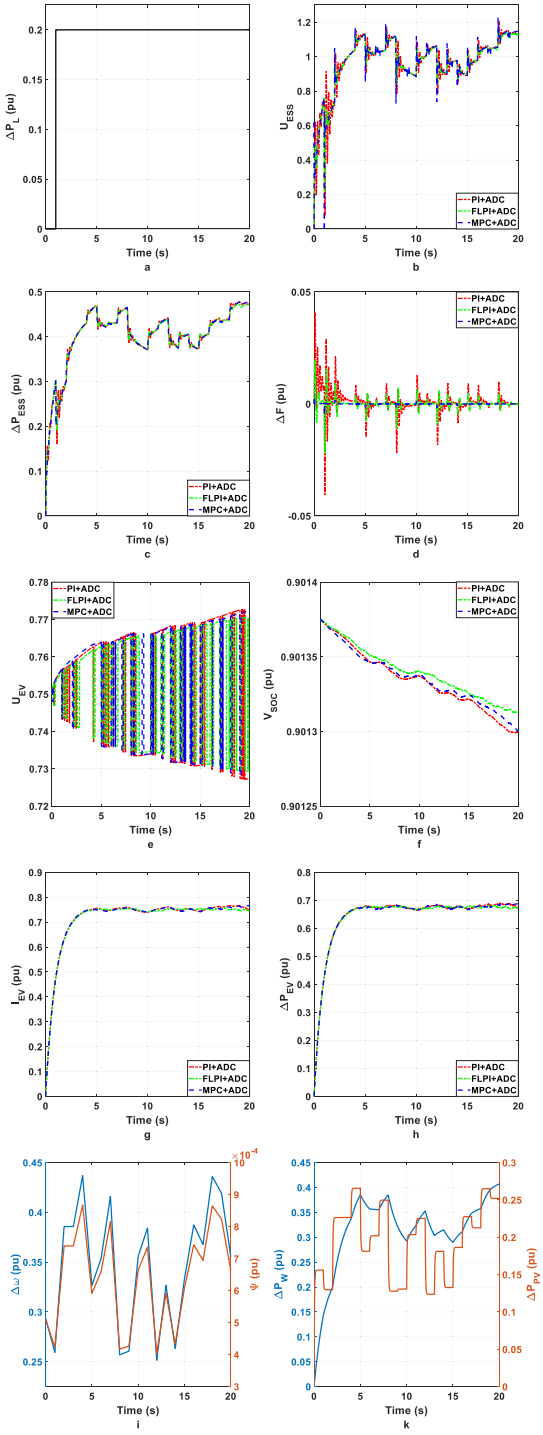

FIGURE 13. The performance results for ESS/EV for load variations with RESs penetration by PI/*ADC*, FPI/*ADC*, and MPC/*ADC* controllers. (a) step-change load variation in p.u. (b) The input signal of ESS. (c) the power of the ESS (d) The frequency response (e) Input single of EV. (f) The voltage of the EV battery. (g) The current of the EV battery. (h) The output power of an EV. (i) The generator speed and the irradiation of the PV cell (k) The wind and the PV output power.

for future utilization therefore the ESS discharge its power until the system becomes stabilized. The first goal of EVBs is to provide the necessary power to fulfill their own needs, which means they should preserve their desired power first and then interact with MG frequency deviations. Here the adaptive droop controller (*ADC*) regulates the output power of EVBs (ΔP_{EV}) according to Δf in order to participate effectively in frequency regulation of the isolated MG. The ΔP_{EV} is uniformly managed by PI $-$ *ADC*, FPI $-$ *ADC*, and MPC $-$ *ADC* as these controllers (PI, FPI, and MPC) don't affect the performance of the *ADC* to regulate the cumulative power of the EVBs. Moreover, *ADC* and optimized MPC reduces the frequency deviations by regulating their respective energy storage in order to bring back the MG frequency to the normal operating position as given in Fig. 13(d).

The damping, overshoot, settling time and the sustainment of the system frequency within the desired limits are not effectively managed by the combination of PI$-$*ADC* and FPI$-$*ADC* controllers.

D. CASE 4

The real-time data of wind speed and solar irradiance is considered beside the random load variations. The ΔP_L varies between 0.15 and 0.75 p.u., the wind speed and the solar irradiance as shown in Fig 14(a), 14(i), and 14(k), respectively.

During huge and sudden load variations, the PI $-$ *ADC* violates the upper and lower limits of Δf. For instant at

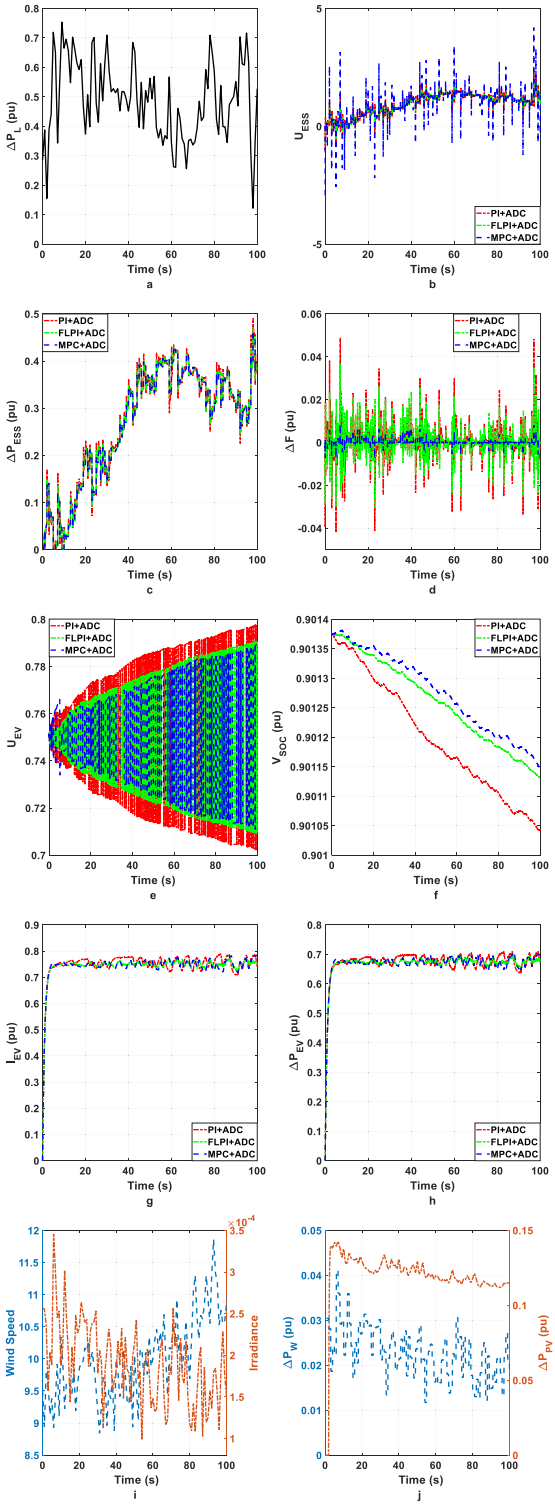

FIGURE 14. The performance results for ESS/EV for load variations with RESs penetration by PI/*ADC*, FPI/*ADC*, and MPC/*ADC* controllers. (a) step-change load variation in p.u. (b) The input signal of ESS. (c) the power of the ESS (d) The frequency response (e) Input single of EV. (f) The voltage of the EV battery. (g) The current of the EV battery. (h) The output power of an EV. (i) The generator speed and the irradiation of the PV cell (k) The wind and the PV output power.

time $t = 2sec$ when the ΔP_L suddenly decrease from 0.72 to o.35 p.u. the PI$-$*ADC* couldn't manage the system frequency properly as the Δf crosses the -0.04 at this instant. Similarly, the optimized FPI and *ADC* combination show better performance than PI$-$*ADC* controllers. However, at time $t = 60sec$, it violates the limits as evident in Fig. 14(d). The combination of optimized MPC $-$ *ADC* controllers shows much better results and good performance regarding damping, overshoot, settling time, and the sustainment of the system frequency within the desired limits.

V. CONCLUSION

In the isolated microgrid (MG) mode of operation, the stability of frequency is a significant control issue. Therefore, this article presented the control techniques that regulate the frequency of isolated MG in an effective manner. The adopted control technique is comprised of proportional integral controller (PI), adaptive droop control (*ADC*), fuzzy logic proportional integral controller (FPI) and model predictive controller (MPC) controller. The system including electric vehicles (EVs), an energy storage system (ESS), a wind turbine, a solar system, and a diesel generator are studied. The PI, FPI, and MPC controllers are used to control the output of the ESS. Whereas, *ADC* is used for regulating the EVs batteries. The impact of load variation on the system's frequency is also analyzed. Meanwhile, the PI, FPI, and MPC controllers' parameters are well-tuned with the help of genetic algorithm optimization in order to enhance the system stability and frequency response under fixed as well as various load variations. Moreover, a high RESs penetration (by wind and solar) is considered to observe their impact on the mentioned controllers' design and, on the frequency of isolated MG. MATLAB/SIMULINK is used as a tool to validate the performance of the presented control techniques on the frequency of isolated MG. The simulation results depict that the frequency deviation is restored effectively with the help of the proposed control techniques. In addition, the performance of MPC $-$ *ADC* controllers are fairly better than the PI$-$*ADC* and FPI$-$*ADC* controllers regarding damping, overshoot, settling time, and the sustainment of the system frequency within the desired limits.

In future works, a single controller will be designed in order to regulate the *SOC* of both ESS and EVs. Moreover, the role of converters which control the wind and solar power will be taken into account in the frequency response model.

REFERENCES

[1] H. Ur Rehman, X. Yan, M. A. Abdelbaky, M. U. Jan, and S. Iqbal, "An advanced virtual synchronous generator control technique for frequency regulation of grid-connected PV system," *Int. J. Electr. Power Energy Syst.*, vol. 125, Feb. 2021, Art. no. 106440.

[2] H. U. Rehman, X. Yan, M. A. Abdelbaky, M. U. Jan, S. Iqbal, A. Masood, T. Egamnazrova, and M. Aurangzeb, "Droop control design based on advanced particle swarm optimization for grid-connected multi PV-VSG," in *Proc. 16th IET Int. Conf. AC DC Power Transmiss. (ACDC)*, 2020, pp. 1–6.

[3] A. Fernández-Guillamón, E. Gómez-Lázaro, E. Muljadi, and Á. Molina-García, "Power systems with high renewable energy sources: A review of inertia and frequency control strategies over time," *Renew. Sustain. Energy Rev.*, vol. 115, Nov. 2019, Art. no. 109369.

[4] C. Zheng, T. Dragicevic, and F. Blaabjerg, "Model predictive control based virtual inertia emulator for an islanded AC microgrid," *IEEE Trans. Ind. Electron.*, early access, Jul. 10, 2020, doi: 10.1109/TIE.2020.3007105.
[5] C. Seneviratne and C. Ozansoy, "Frequency response due to a large generator loss with the increasing penetration of wind/PV generation—A literature review," *Renew. Sustain. Energy Rev.*, vol. 57, pp. 659–668, May 2016.
[6] X. Luo, J. Wang, J. Wojcik, J. Wang, D. Li, M. Draganescu, Y. Li, and S. Miao, "Review of voltage and frequency grid code specifications for electrical energy storage applications," *Energies*, vol. 11, no. 5, p. 1070, Apr. 2018.
[7] A. Nieto, V. Vita, L. Ekonomou, and N. E. Mastorakis, "Economic analysis of energy storage system integration with a grid connected intermittent power plant, for power quality purposes," *Technology*, vol. 2, p. 5, Jan. 2016.
[8] N. Banol Arias, S. Hashemi, P. B. Andersen, C. Traeholt, and R. Romero, "Distribution system services provided by electric vehicles: Recent status, challenges, and future prospects," *IEEE Trans. Intell. Transp. Syst.*, vol. 20, no. 12, pp. 4277–4296, Dec. 2019.
[9] S. Iqbal, A. Xin, M. U. Jan, M. A. Abdelbaky, H. U. Rehman, S. Salman, S. A. A. Rizvi, and M. Aurangzeb, "Aggregation of EVs for primary frequency control of an industrial microgrid by implementing grid regulation & charger controller," *IEEE Access*, vol. 8, pp. 141977–141989, 2020.
[10] S. Iqbal, A. Xin, M. U. Jan, S. Salman, A. U. M. Zaki, H. U. Rehman, M. F. Shinwari, and M. A. Abdelbaky, "V2G strategy for primary frequency control of an industrial microgrid considering the charging station operator," *Electronics*, vol. 9, no. 4, p. 549, Mar. 2020.
[11] Y. Bai, J. Li, H. He, R. C. D. Santos, and Q. Yang, "Optimal design of a hybrid energy storage system in a plug-in hybrid electric vehicle for battery lifetime improvement," *IEEE Access*, vol. 8, pp. 142148–142158, 2020.
[12] D. H. Tungadio, R. C. Bansal, M. W. Siti, and N. T. Mbungu, "Predictive active power control of two interconnected microgrids," *Technol. Econ. Smart Grids Sustain. Energy*, vol. 3, no. 1, p. 3, Dec. 2018.
[13] A. Annamraju and S. Nandiraju, "Robust frequency control in a renewable penetrated power system: An adaptive fractional order-fuzzy approach," *Protection Control Mod. Power Syst.*, vol. 4, no. 1, p. 16, Dec. 2019.
[14] M. F. M. Arani and Y. A.-R.-I. Mohamed, "Cooperative control of wind power generator and electric vehicles for microgrid primary frequency regulation," *IEEE Trans. Smart Grid*, vol. 9, no. 6, pp. 5677–5686, Nov. 2018.
[15] T. Kerdphol, F. S. Rahman, Y. Mitani, M. Watanabe, and S. Kufeoglu, "Robust virtual inertia control of an islanded microgrid considering high penetration of renewable energy," *IEEE Access*, vol. 6, pp. 625–636, 2018.
[16] T. Kerdphol, M. Watanabe, K. Hongesombut, and Y. Mitani, "Self-adaptive virtual inertia control-based fuzzy logic to improve frequency stability of microgrid with high renewable penetration," *IEEE Access*, vol. 7, pp. 76071–76083, 2019.
[17] T. Kerdphol, Y. Mitani, and K. Hongesombut, "Intelligent determination of electric vehicle size for microgrid frequency stabilization using artificial neural network," in *Proc. 8th Thailand-Jpn. Int. Acad. Conf.*, Bangkok, Thailand, 2016, pp. 1–6.
[18] J. Alcalá-Fdez, R. Alcalá, M. J. Gacto, and F. Herrera, "Learning the membership function contexts for mining fuzzy association rules by using genetic algorithms," *Fuzzy Sets Syst.*, vol. 160, no. 7, pp. 905–921, Apr. 2009.
[19] M. Patrascu and A. Ion, "Evolutionary modeling of industrial plants and design of PID controllers," in *Nature-Inspired Computing for Control Systems*. Cham, Switzerland: Springer, 2016, pp. 73–119.
[20] P. Dolezel and J. Mares, "Self tuning PID control using genetic algorithm and artificial neural networks," in *Proc. ASR Instrum. Control*, 2009, pp. 33–39.
[21] C.-C. Kao, C.-W. Chuang, and R.-F. Fung, "The self-tuning PID control in a slider–crank mechanism system by applying particle swarm optimization approach," *Mechatronics*, vol. 16, no. 8, pp. 513–522, Oct. 2006.
[22] J. Hu and A. Lanzon, "Distributed finite-time consensus control for heterogeneous battery energy storage systems in droop-controlled microgrids," *IEEE Trans. Smart Grid*, vol. 10, no. 5, pp. 4751–4761, Sep. 2019.
[23] D. Lamsal, V. Sreeram, Y. Mishra, and D. Kumar, "Smoothing control strategy of wind and photovoltaic output power fluctuation by considering the state of health of battery energy storage system," *IET Renew. Power Gener.*, vol. 13, no. 4, pp. 578–586, Mar. 2019.
[24] F. Díaz-González, A. Sumper, O. Gomis-Bellmunt, and R. Villafáfila-Robles, "A review of energy storage technologies for wind power applications," *Renew. Sustain. Energy Rev.*, vol. 16, no. 4, pp. 2154–2171, May 2012.
[25] F. Zhang, A. Fu, L. Ding, and Q. Wu, "MPC based control strategy for battery energy storage station in a grid with high photovoltaic power penetration," *Int. J. Electr. Power Energy Syst.*, vol. 115, Feb. 2020, Art. no. 105448.
[26] S. Izadkhast, P. Garcia-Gonzalez, P. Frias, and P. Bauer, "Design of plug-in electric vehicle's frequency-droop controller for primary frequency control and performance assessment," *IEEE Trans. Power Syst.*, vol. 32, no. 6, pp. 4241–4254, Nov. 2017.
[27] K. Kaur, M. Singh, and N. Kumar, "Multiobjective optimization for frequency support using electric vehicles: An aggregator-based hierarchical control mechanism," *IEEE Syst. J.*, vol. 13, no. 1, pp. 771–782, Mar. 2019.
[28] M. U. Jan, A. Xin, M. A. Abdelbaky, H. U. Rehman, and S. Iqbal, "Adaptive and fuzzy PI controllers design for frequency regulation of isolated microgrid integrated with electric vehicles," *IEEE Access*, vol. 8, pp. 87621–87632, 2020.
[29] M. U. Jan, A. Xin, S. Iqbal, M. A. Abdelbaky, H. U. Rehman, T. Egamnazrova, S. A. A. Rizvi, and S. Salman, "Frequency regulation of an isolated micro-grid integrated with electric vehicles using adaptive and fuzzy PI controllers," in *Proc. 16th IET Int. Conf. AC DC Power Transmiss. (ACDC)*, 2020, pp. 1–6.
[30] H. Zhu, S. A. Z. Ahmed, M. A. Alfakih, M. A. Abdelbaky, A. R. Sayed, and M. A. A. Saif, "Photovoltaic failure diagnosis using sequential probabilistic neural network model," *IEEE Access*, vol. 8, pp. 220507–220522, 2020.
[31] I. Houssamo, F. Locment, and M. Sechilariu, "Maximum power tracking for photovoltaic power system: Development and experimental comparison of two algorithms," *Renew. Energy*, vol. 35, no. 10, pp. 2381–2387, Oct. 2010.
[32] X. Ma, Y. Wang, and J. Qin, "Generic model of a community-based microgrid integrating wind turbines, photovoltaics and CHP generations," *Appl. Energy*, vol. 112, pp. 1475–1482, Dec. 2013.
[33] M. A. Abdelbaky, X. Liu, and D. Jiang, "Design and implementation of partial offline fuzzy model-predictive pitch controller for large-scale wind-turbines," *Renew. Energy*, vol. 145, pp. 981–996, Jan. 2020.
[34] M. A. Abdelbaky, X. Liu, and X. Kong, "Wind turbines pitch controller using constrained fuzzy-receding horizon control," in *Proc. Chin. Control Decis. Conf. (CCDC)*, Jun. 2019, pp. 236–241.
[35] G. Mom, *The Electric Vehicle: Technology and Expectations in the Automobile Age*. Baltimore, MD, USA: JHU Press, 2013.
[36] J. R. Pillai and B. Bak-Jensen, "Integration of vehicle-to-grid in the western Danish power system," *IEEE Trans. Sustain. Energy*, vol. 2, no. 1, pp. 12–19, Jan. 2010.
[37] D.-I. Stroe, V. Knap, M. Swierczynski, A.-I. Stroe, and R. Teodorescu, "Operation of a grid-connected lithium-ion battery energy storage system for primary frequency regulation: A battery lifetime perspective," *IEEE Trans. Ind. Appl.*, vol. 53, no. 1, pp. 430–438, Jan. 2017.
[38] E. Kayacan and M. A. Khanesar, *Fuzzy Neural Networks for Real Time Control Applications*, vol. 720. Oxford, U.K.: Butterworth-Heinemann, 2016.
[39] L. Wang, *Model Predictive Control System Design and Implementation Using MATLAB*. London, U.K.: Springer, 2009.
[40] P. J. Fleming and R. C. Purshouse, "Evolutionary algorithms in control systems engineering: A survey," *Control Eng. Pract.*, vol. 10, no. 11, pp. 1223–1241, Nov. 2002.
[41] B. O. Bush, J.-P. Hosom, A. Kain, and A. Amano-Kusumoto, "Using a genetic algorithm to estimate parameters of a coarticulation model," in *Proc. 12th Annu. Conf. Int. Speech Commun. Assoc.*, 2011, pp. 1–4.
[42] C.-F. Huang, "A hybrid stock selection model using genetic algorithms and support vector regression," *Appl. Soft Comput.*, vol. 12, no. 2, pp. 807–818, Feb. 2012.
[43] M. A. Abdelbaky, H. M. Emara, M. I. El-Hawwary, A. Bahgat, and X. Liu, "Implementation of fractional-order PID controller using industrial DCS with experimental validation," in *Proc. IEEE 4rd Conf. Energy Internet Energy Syst. Integr. (EI)*, Wuhan, China, 2020, pp. 7–12.
[44] Q. Tao, X. Liu, and M. Xue, "A dynamic genetic algorithm based on continuous neural networks for a kind of non-convex optimization problems," *Appl. Math. Comput.*, vol. 150, no. 3, pp. 811–820, Mar. 2004.
[45] H. U. Rehman, X. Yan, M. A. Abdelbaky, M. U. Jan, A. R. Sayed, S. A. Zaki, and S. Iqbal, "Frequency regulation and optimization of microgrid system with multi PV-VSG using advanced droop controller," in *Proc. IEEE 4rd Conf. Energy Internet Energy Syst. Integr. (EI)*, Wuhan, China, 2020, pp. 1–6.

MISHKAT ULLAH JAN received the B.Sc. degree in electrical engineering from the University of Engineering and Technology at Bannu, Bannu, Pakistan, in 2010, and the M.S. degree in electrical engineering from the CECOS University of IT and Emerging Sciences, Peshawar, Pakistan, in 2014. He is currently pursuing the Ph.D. degree in electrical engineering with North China Electric Power University, Beijing, China. From 2010 to 2011, he has worked as a Trainee Engineer under the National Internship Program at Sarhad Hydel Development Organization, Pakistan. From 2014 to 2015, he has worked as a Research Associate with CECOS University. His research interests include power system stability, frequency regulation, and energy management of microgrid.

AI XIN (Member, IEEE) was born in 1964. He received the B.S. degree from the Nanjing Institute of Technology (now Southeast University), Nanjing, China, in 1985, the M.S. degree from the China Electric Power Research Institute, Beijing, China, in 1988, and the Ph.D. degree from North China Electric Power University (NCEPU), Beijing, in 1999, all in electrical engineering. He was a Senior Research Scholar with Brunel University, London, U.K., in 2003. He was the Director of the Institute of Power Systems, NCEPU, where he was engaged in research and teaching on power system and automation. He is currently a Professor and a Doctoral Tutor with the School of Electrical and Electronic Engineering, NCEPU. His current research interests include power system analysis and control, and transactive energy.

HASEEB UR REHMAN received the B.S. degree in electrical engineering from the University of Engineering and Technology at Bannu, Bannu, Pakistan, in 2010, and the M.S. degree in electrical engineering from the University of Engineering and Technology at Peshawar, Peshawar, in 2016. He is currently pursuing the Ph.D. degree in electrical engineering with North China Electric Power University, Beijing, China.

From 2012 to 2017, he has worked as an Engineer Distribution with Sui Northern Gas Pipeline Ltd., Pakistan. His research interests include the integration of renewable energy source in microgrid, frequency stability, and control of microgrid through virtual synchronous generator.

MOHAMED ABDELKARIM ABDELBAKY received the B.Sc. and M.Sc. degrees in electrical engineering from Cairo University, Cairo, Egypt, in 2013 and 2016, respectively. He is currently pursuing the Ph.D. degree with the School of Control and Computer Engineering, North China Electric Power University, Beijing, China.

He has joined the Department of Electrical Power and Machines Engineering, Cairo University, as an Associate Lecturer, in 2016. His current research interests include nonlinear model predictive control and its applications in power plants.

SHEERAZ IQBAL received the B.E. degree in telecommunication engineering from Allama Iqbal Open University, Islamabad, Pakistan, in 2010, the M.S. degree in electronic engineering from International Islamic University, Islamabad, in 2014, and the Ph.D. degree from the School of Electrical and Electronic Engineering, North China Electric Power University, China, in 2020. He has served as a Lecturer with the Department of Electrical Engineering, University of Azad Jammu and Kashmir, Muzaffarabad, Pakistan, from 2014 to 2017. He is currently an Assistant Professor with the University of Azad Jammu and Kashmir. His research interests include primary frequency control, MG energy management, and electric vehicles integration in industrial MG.

MUHAMMAD AURANGZEB received the B.S. degree from the Department of Electrical Engineering, COMSATS University, Abbottabad, Pakistan, in 2013, and the M.S. degree in power system and automation from Hohai University, Nanjing, China. He is currently pursuing the Ph.D. degree in electrical engineering with North China Electric Power University, Beijing, China. His research interests include power system stability, power system protection, electric vehicles scheduling, and electricity markets.